This is an open access article published under an ACS AuthorChoice License, which permits copying and redistribution of the article or any adaptations for non-commercial purposes.

Downloaded via NANYANG TECHNOLOGICAL UNIV on April 22, 2019 at 05:49:46 (UTC).
See https://pubs.acs.org/sharingguidelines for options on how to legitimately share published articles.

ARTICLE

Bimodal Tumor-Targeting from Microenvironment Responsive Hyaluronan Layer-by-Layer (LbL) Nanoparticles

Erik C. Dreaden,[†,‡] Stephen W. Morton,[†,‡] Kevin E. Shopsowitz,[†,‡] Jae-Hyeok Choi,[⊥,∥] Zhou J. Deng,[†,‡] Nam-Joon Cho,[⊥,∥,#] and Paula T. Hammond[†,‡,§,*]

[†]Koch Institute for Integrative Cancer Research, [‡]Department of Chemical Engineering, and [§]Institute for Soldier Nanotechnologies, Massachusetts Institute of Technology, 500 Main Street, Cambridge, Massachusetts 02142, United States and [⊥]School of Materials Science and Engineering, [∥]Centre for Biomimetic Sensor Science, and [#]School of Chemical and Biomedical Engineering, Nanyang Technological University, 639798 Singapore

ABSTRACT Active targeting of nanoscale drug carriers can improve tumor-specific delivery; however, cellular heterogeneity both within and among tumor sites is a fundamental barrier to their success. Here, we describe a tumor microenvironment-responsive layer-by-layer (LbL) polymer drug carrier that actively targets tumors based on two independent mechanisms: pH-dependent cellular uptake at hypoxic tumor pH and hyaluronan-directed targeting of cell-surface CD44 receptor, a well-characterized biomarker for breast and ovarian cancer stem cells. Hypoxic pH-induced structural reorganization of hyaluronan-LbL nanoparticles was a direct result of the nature of the LbL electrostatic complex, and led to targeted cellular delivery *in vitro* and *in vivo*, with effective tumor penetration and uptake. The nanoscale drug carriers selectively bound CD44 and diminished cancer cell migration *in vitro*, while co-localizing with the CD44 receptor *in vivo*. Multimodal targeting of LbL nanoparticles is a powerful strategy for tumor-specific cancer diagnostics and therapy that can be accomplished using a single bilayer of polyamine and hyaluronan that, when assembled, produce a dynamic and responsive cell−particle interface.

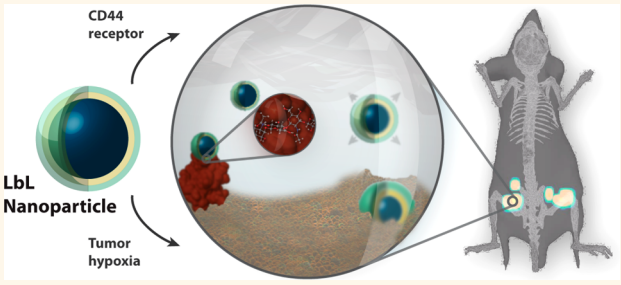

KEYWORDS: self-assembly · nanomaterials · nanomedicine · polymer engineering · controlled delivery

Nanoscale drug delivery is an attractive option for cancer therapeutics that exhibit poor pharmacokinetics,[1] dose-limiting toxicities, or chemical instability.[2] This strategy typically improves tumor-specific delivery through either size-dependent "passive" targeting[3,4] and/or "active" targeting that can be ligand-directed[5] or stimuli-responsive.[6] While active targeting often augments tumor cell killing, its efficacy is intrinsically limited by cellular heterogeneity that exists both within and among tumors.[7−9] Genetic diversity within breast tumors, for example, is known to be associated with both tumor stage and subtype in breast carcinoma.[10] Similarly, diversity within the subclonal structure of esophageal lesions is known to predict progression to malignancy.[11] Following metastasis, as many as 24−38% of breast, lung, and melanoma cancer patients exhibit differential expression of biomarkers that predicate treatment response (*i.e.*, amplified *HER2*, mutant *EGFR*, and mutant *BRAF*, respectively).[12] Tumor heterogeneity is a fundamental challenge to the success of actively targeted nanoscale drug delivery, and vehicles capable of multimodal active targeting are urgently needed.

Layer-by-Layer (LbL) nanoparticles are an emerging class of self-assembled polymer drug carrier that addresses several challenges in the delivery of small molecule therapeutics and imaging agents.[13−21] These modular structures consist of (i) a functional nanoparticle core, (ii) a multilayered polyelectrolyte shell, and (iii) an exterior tumor-targeting stealth layer. The core consists of drug-loaded polymer nanoparticles,[22−25] liposomes,[26,27] multimeric RNA,[28]

* Address correspondence to hammond@mit.edu.

Received for review May 26, 2014 and accepted August 6, 2014.

Published online August 06, 2014
10.1021/nn502861t

© 2014 American Chemical Society

or a range of organic/inorganic nanoscale materials and imaging agents (*i.e.*, quantum dots,[20] silica,[29] gold,[20] hydroxyapatite,[30] or iron oxide[31]). The multilayered shell can include hierarchically assembled polymers, proteins, small molecules, or nucleic acids that exhibit complementary charge/bonding interactions.[32,33] In prior work, we demonstrated that LbL nanoparticle architectures can achieve long systemic circulation (elimination $t_{1/2} \sim 28$ h),[26] low off-target delivery (10−15% ID/g liver),[20] and active tumor targeting,[19] and enhanced the *in vivo* stability of therapeutic RNA for efficacious synergistic siRNA/drug combination therapy,[26,28] or incorporate nanoparticle cores containing diagnostic imaging agents[23] and cytotoxic chemotherapeutics.[26,27] Here, we engineer a novel LbL nanoparticle architecture that actively targets solid tumors through two independent mechanisms: selective binding to cell-surface CD44 receptor and acid-induced cellular delivery at hypoxic tumor pH. This approach allows for the creation of nanoparticles that respond to the tumor microenvironment in two unique ways, thus greatly enhancing targeting and uptake. Rather than employing nondegradable neutral polymers such as poly(ethylene glycol), synthetic ligand attachment, or complex linker chemistry, we accomplish an intrinsic responsive behavior through the simple use of biologically derived weak polyelectrolytes in a self-assembled thin film.

2D LbL films assembled from partially ionized or "weak" polyelectrolytes are well-known to exhibit dynamic structure and stability with respect to pH compared with their strong polyelectrolyte counterparts.[34−36] For example, dramatic shifts in adsorbed layer thickness, surface morphology, and effective ionic cross-link density have been observed due to thermodynamic trade-offs and weak Coulombic interactions between nearest-neighbor proton binding sites.[36] The hypoxic microenvironment of solid tumors also exhibit a narrow gradient in pH; poor blood perfusion and rapid metabolic consumption of oxygen results in a drop in pH from 7.4 (normoxic) to <6.6 in distances as short as 150 μm from the vessel wall,[37] providing an environment that can select for and host aggressive and metastatic cell phenotypes.[38] One of the challenges in nanoparticle design for cancer treatment is their infiltration and penetration through the stroma and into tumor tissues, and selective uptake of nanoparticles within the tumor tissue.

We hypothesized that LbL nanoparticle architectures incorporating functional biopolymers that, themselves, are weak polyelectrolytes may achieve both receptor-targeting *and* pH-triggered engagement of and delivery to solid tumors without the need for ligand coupling chemistries, active proteins, or stealth layers that can introduce potential issues with compatibility, immune response, or blood half-life. To this end, we selected a weak polyamine, poly(L-lysine), which is a synthetic polypeptide from a natural amino acid, and a complementary weak polyacid, hyaluronan (HA), which is a native extracellular matrix polysaccharide, to serve as functional components of this dual-targeting LbL drug carrier. While both polyelectrolytes are biocompatible pharmaceutical excipients (*i.e.*, benzylpenicilloyl polylysine), hyaluronan, also known as hyaluronic acid or HA, is unique in that it also exhibits protein-repellent behavior and is an active component in many postsurgical adhesion barriers.[39] Importantly, hyaluronan is the endogenous ligand for cell-surface receptor CD44, a well-characterized biomarker for breast and ovarian carcinoma cells with tumor-initiating,[40] drug-resistant,[41] and stem-like phenotype[42,43] that can be used to target these tumors.[44−46] A unique capability introduced with LbL nanofilms containing hyaluronan is the potential to tune its charge interactions with an underlying polyamine to produce a dense and compact charged repulsive, sterically shielding layer at blood pH that can convert to a swollen neutral layer that readily engages cells at hypoxic tissue pH.

RESULTS AND DISCUSSION

Dual-targeting hyaluronan-LbL architectures (Figure 1), consisting of only 2 layers, or 1 bilayer repeat, were assembled onto model drug carriers (fluorescent polystyrene nanoparticles) *via* sequential adsorption and centrifugation from solutions of aqueous hyaluronan and poly(L-lysine), as described previously.[20] Figure 2a,b illustrates the gradual increase in hydrodynamic size and corresponding shift in surface charge of the nanoparticles during the LbL assembly process, yielding particles 135 ± 4 nm in hydrodynamic diameter and −33 ± 1 mV in zeta potential. Transmission electron

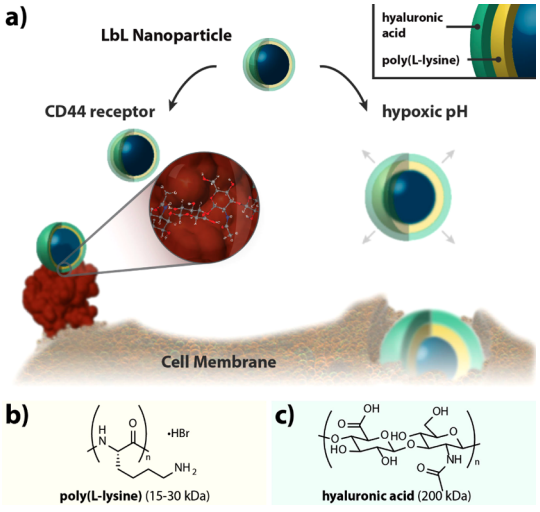

Figure 1. Hyaluronan Layer-by-Layer (LbL) nanoparticles actively target hypoxic tumor pH and cancer stem cell receptor CD44. (a) Schematic illustrating bimodal tumor-targeted delivery. (b) Polycation and (c) polyanion components of the LbL nanoparticle. CD44 protein structure in (a) is rendered from biological assembly 1 of PDB ID 1UUH.

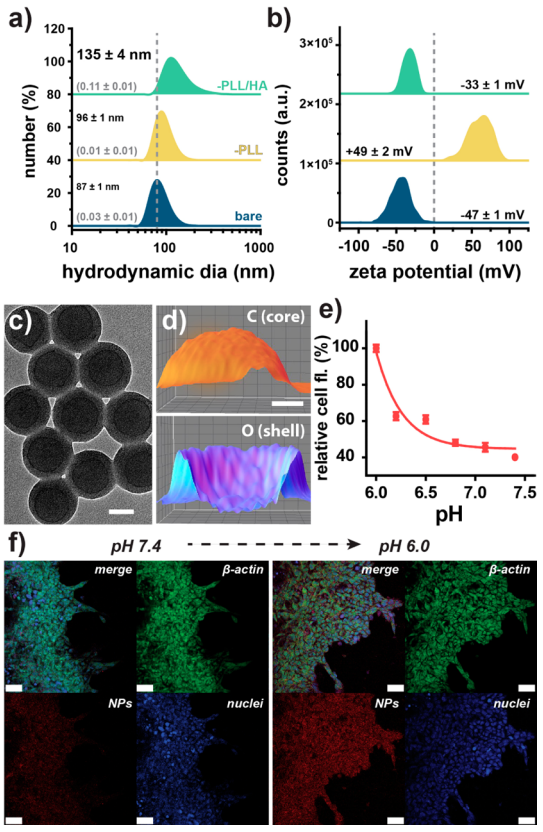

Figure 2. pH-responsive hyaluronan-LbL nanoparticles target hypoxic tumor pH *in vitro*. (a) Increase in hydrodynamic size and (b) concomitant shift in surface charge during LbL assembly onto mock fluorescent drug carriers as measured by photon correlation spectroscopy and laser Doppler electrophoresis, respectively. (c) Transmission electron microscopy (TEM) of the subsequent hyaluronan-LbL nanoparticle assemblies and (d) a cross-sectional elemental mapping reconstruction of an individual LbL nanoparticle as imaged by energy-filtered TEM (EFTEM). (e) pH-dependent cellular delivery of hyaluronan-LbL nanoparticles to Hep G2 hepatocyte cells as measured by flow cytometry (t = 3 h). (f) Confocal fluorescence micrographs of hypoxic pH-augmented cellular delivery of hyaluronan-LbL nanoparticles (red) to 3D Hep G2 tumor spheroids. Measurements in (a and b) were obtained in deionized water. Values in parentheses in (a) represent polydispersity index. Error bars represent SD of three technical replicates. Scale bar is (c) 50 nm, (d) 20 nm, and (f) 20 μm.

micrographs (Figure 2c) and cross-sectional 3D renderings of energy-filtered transmission electron microscopy (TEM) images (EFTEM, Figure 2d) confirmed structural partitioning between the carbon-rich polystyrene nanoparticle core and the oxygen-rich LbL multilayered shell. Notably, thickness increases from the terminal HA layer (20 ± 2 nm) appeared larger than typically observed from other weak and strong polyelectrolytes (*ca.* 4−5 nm).[23] In solution, HA's conformation is composed of a combination of random coil and helical structures, the latter of which can self-associate and entangle through interactions between outer hydrophobic pocket regions of the helices.[47] In LbL films, Burke *et al.* find that HA undergoes an significant increase in secondary conformational ordering and intermolecular H bonding.[48] We hypothesize that surface-induced helical ordering of HA on LbL nanoparticles results in increased self-association between surface-bound HA chains that leads to non-surface-limited coverages observed here. HA-LbL nanoparticles were well-dispersed (PDI 0.11 ± 0.01) and exhibited few (<1.2%) dimers and no (0%) higher order aggregates. The thick layer of HA on the exterior surface provides an enhanced degree of hydration due to the waters of hydration of HA and the availability of a dense number of flexible HA chains on the nanoparticle surface that contribute to steric stability.

Hypoxic pH-Mediated Uptake. We assessed pH-dependent cell binding/uptake of the hyaluronan-LbL nanoparticles by flow cytometry of Hep G2 human hepatocyte cells. Figure 2e illustrates a 2.4-fold increase in nanoparticle-associated cellular fluorescence as extracellular pH is reduced from normoxic (7.4) to hypoxic pH (6.0) during nanoparticle incubation (3 h). Interestingly, nonspecific targeting of the hyaluronan-nanoparticles at pH 7.4 was 15-fold lower than that from a related acid-labile PEG-LbL architecture with a pH-sensitive iminobiotin linker previously designed in our group to release a PEG shielding layer and "unveil" positively charged surfaces (Supporting Information Figure S1a).[19] These findings are consistent with the notion that mucopolysaccharide-coated (*i.e.*, HA-terminal) surfaces can exhibit antifouling behavior to prevent protein opsonization.[49] Hypoxic pH-specific delivery of the hyaluronan-LbL architecture (pH 6.0 v 7.4) was likewise improved 2.5-fold relative to the previous iminobiotin architecture (Supporting Information Figure S1b) in Hep G2 cells, indicating enhanced cellular delivery at pH values reflective of the hypoxic tumor microenvironment. Delivery of the hyaluronan-LbL nanoparticles into 3D tumor spheroids was also investigated by confocal fluorescence microscopy of Hep G2 hepatocyte and breast adenocarcinoma cell nodules. We observed both high tumor penetration (Supporting Information Figure S2) and hypoxic pH-responsive delivery (Figure 2f) of hyaluronan-LbL nanoparticles into 3D tumor spheroids (3 h), important properties necessary for efficient penetration throughout the often compacted (*i.e.*, desmoplastic) tumor stroma.[50]

We next investigated pH-dependent structural changes in the hyaluronan-LbL architecture by TEM, photon correlation spectroscopy, laser Doppler electrophoresis, quartz crystal microbalance-dissipation (QCM-D), and contact angle measurements. Low electron dose TEM images of particles incubated in pH 7.4 and 6.0 buffer indicate significant (*ca.* 3.1-fold) swelling of the LbL polymer shell at hypoxic tumor pH (Figure 3a), findings corroborated by DLS measurements that indicate a half maximal increase in hydrodynamic size at *ca.* pH 6.8 (Figure 3b). This hydrodynamic shell thickness increase agreed well with that observed by TEM, also swelling 3.1-fold from 24 ± 8 nm

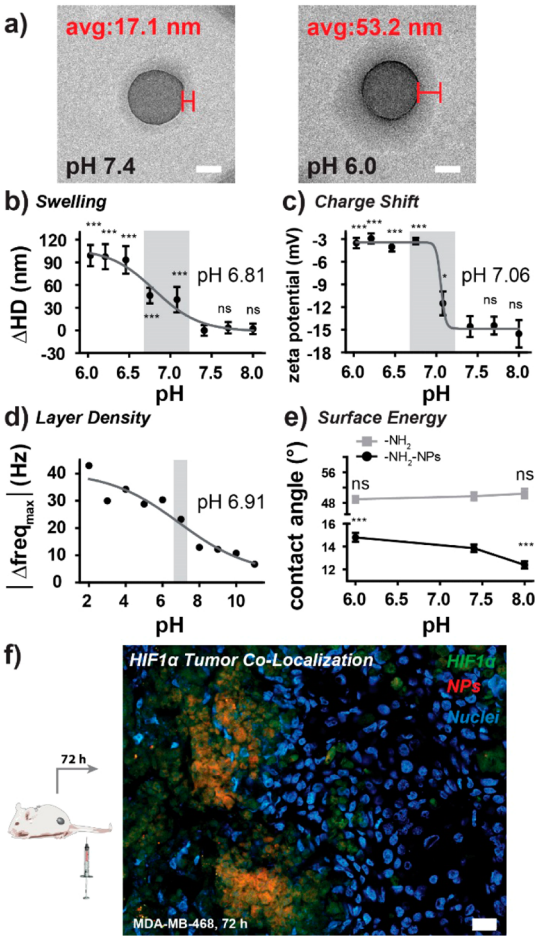

Figure 3. Hypoxic pH-induced structural reorganization of hyaluronan-LbL nanoparticles and *in vivo* hypoxic tumor-targeting. (a) Low electron-dose TEM illustrating pH-dependent LbL bilayer swelling. (b) pH-dependent hydrodynamic swelling and (c) loss of stabilizing surface charge as measured by photon correlation spectroscopy and laser Doppler electrophoresis, respectively. (d) Quartz crystal microbalance dissipation (QCM-D) tracking of pH-dependent hyaluronan adsorption onto amine-modified Au. (e) Contact angle measurements of substrate-immobilized hyaluronan-LbL nanoparticles demonstrating hypoxic pH-dependent decreased surface energy at hypoxic pH. (f) *In vivo* tumor co-localization of hyaluronan-LbL nanoparticles (red) with hypoxia-inducible factor 1 α (HIF1α, green) in subcutaneous triple-negative breast carcinoma tumor xenografts (iv). Measurements in (b and c) were obtained in phosphate buffered saline. Nominal hypoxic tumor pH ranges are shaded in (b–d). Error represents SD of three technical replicates. Scale bar is (a) 50 nm and (f) 10 μm. Statistical significance in (e) is indicated relative to pH 7.4 from the same surface. Not significant (ns).

at pH 7.4 to 74 ± 15 nm at pH 6.0. Zeta potential measurements (Figure 3c) show that pH-dependent swelling is also accompanied by a neutralization of stabilizing surface charge, which drops to an equilibrium value of approximately −3 mV at below *ca.* pH 7.06. QCM-D measurements of hyaluronan adsorption onto amine-modified Au (Figure 3d; Supporting Information Figure S3) likewise suggest a highly pH-dependent assembly process with half maximal frequency shift observed at *ca.* pH 6.91. Contact angle measurements from nanoparticles immobilized on silicon substrates (Figure 3e) similarly support hypoxic pH-induced rearrangements at the surface, as indicated by a statistically significant increase in contact angle with decreasing pH (corresponding to decreased apparent surface energy). These pH-dependent changes in layer thickness, as well as QCM-D and contact angle measurements are consistent with prior reports of planar LbL film assemblies of weak polyacids and polyamines[36,48,51] and suggest that PLL/HA-LbL nanoparticles undergo a pH-dependent structural transition at hypoxic tumor pH (*i.e.*, 6.8 to 7.0) where swelling, loss of anionic charge, and decreased surface energy correlate with increased cell uptake *in vitro*.

Notably, the pK_a of hyaluronic acid in solution is reported to be approximately 3.0 and that of poly(L-lysine) is about 10. A layer of HA alone, thus, would not be anticipated to undergo significant changes in charge at hypoxic pH. In contrast, polyelectrolyte multilayers create controlled complexes that can exhibit acid–base equilibria that are tuned by assembly pH and ionic strength.[34,51] Multilayers of poly(allyl amine) hydrochloride and hyaluronic acid, for example,[52] exhibit dynamic shifts in HA acid dissociation equilibrium, surface roughness, and multilayer swelling as a function of assembly pH. These changes are attributed to a reduction in the apparent acid and base character of the HA and PLL, respectively, due to charge compensation between partially ionized side chains of these "weak" polyelectrolytes following pH-dependent adsorption, as well as assembly induced secondary structure formation that disfavors proton exchange. Such polyelectrolyte assemblies exhibit a unique pK_a that is characteristic of the resulting polyion blend and its assembly conditions. We hypothesize that augmented cellular delivery of the nanoparticles, which is known to increase with increasing surface roughness and/or loss of anionic surface charge,[53] occurs as a result of the previously described pH-dependent structural changes. The swelling of the bilayer may further enhance cell uptake by altering the effective modulus of the nanoparticle and enabling less sterically hindered engagement of the hyaluronic acid groups on the surface of the hydrated outer layer.

Having established hypoxic pH-responsive behavior *in vitro*, we also asked whether hyaluronan-LbL nanoparticles preferentially target tumor hypoxia *in vivo*. Indeed, immunofluorescence microscopy of excised tumor sections indicated a high degree of particle co-localization with hypoxia-inducible factor 1 α (HIF1α)[54] in MDA-MB-468 subcutaneous xenografts following iv tail vein injection in mice (72 h, Figure 3f). Co-localization with HIF1α, a classical oxygen-regulated transcription factor, suggests that HA-LbL nanoparticles preferentially localize in tumor tissues with low pO_2 (*i.e* , <14 mmHg).[54]

Together with the previous results, these data support that hyaluronan-LbL nanoparticles undergo cell

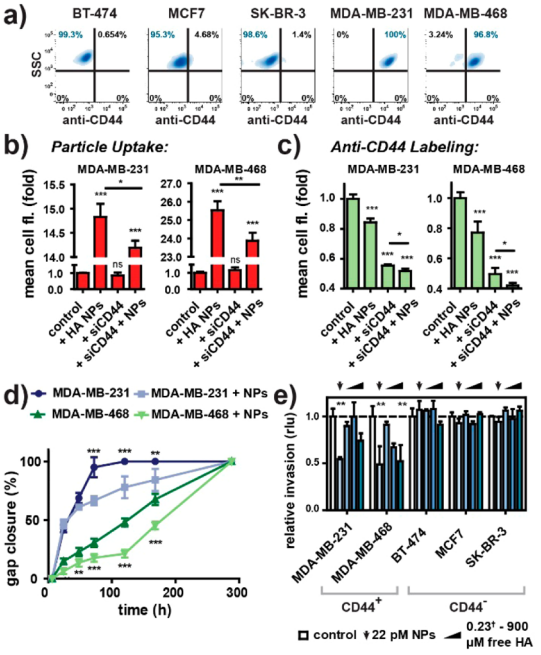

Figure 4. Hyaluronan-LbL nanoparticles target cancer stem cell receptor CD44 and selectively decrease *in vitro* migration/invasion. (a) CD44 receptor expression in panel of breast carcinoma cells, as measured by antibody-labeling and flow cytometry. (b) CD44-specific nanoparticle delivery is decreased following receptor knockdown triple-negative breast carcinoma cells as measured by flow cytometry. (c) Hyaluronan-LbL nanoparticles and CD44 antibodies competitively bind cell-surface receptor CD44 in MDA-MB-231 and -468 breast carcinoma cells as measured by flow cytometry. (d) Dual-targeting hyaluronan-LbL nanoparticles diminish both 2D cell migration and (e) 3D collagen gel transwell invasion in a CD44 receptor-selective manner (Supporting Information Figures S3 and S4). Error represents SD of (b–d) three technical and (e) three biological replicates. Dagger symbol (†) in (e) denotes LbL assembly buffer-equivalent concentrations of HA.

uptake-promoting chemical and structural changes over a narrow range in pH that is well-suited for hypoxic tumor targeting. This hypoxic pH-responsive behavior is characterized by hydrodynamic swelling, a loss in stabilizing surface charge, and a decrease in apparent surface energy that correlates with augmented cellular delivery to both 2D and 3D cell cultures, as well as *in vivo* co-localization with hypoxia-inducible factor 1 α in murine tumor models of triple-negative breast carcinoma. The loss of negative charge and slight increase in hydrophobicity of these nanoparticles leads to a significantly increased nonspecific uptake by cells within the local tumor microenvironment.

Role of CD44 Targeting. Given that these LbL nanoparticles are surface-functionalized with hyaluronan, the endogenous ligand for cell-surface receptor CD44, we investigated receptor-specific interactions mediated by these particles in a panel of breast carcinoma cells reflecting luminal, $HER2^+$, and triple-negative (basal) molecular subtypes of the disease (Figure 4a). Note that the previous pH-dependent targeting experiments (above) were performed using a hepatocyte cell line that does not express the CD44 receptor.[55] Consistent with known expression profiles of basal-like breast carcinomas,[43] MDA-MB-231 and MDA-MB-468 cells express high levels of CD44 *in vitro*. Flow cytometry measurements of particle binding/uptake in these cells (pH 7.4, 3 h) indicated a fractional but significant contribution from CD44; this enhanced delivery was abrogated following siRNA-specific silencing of the receptor (Figure 4b), demonstrating the dependence of this behavior on CD44 binding and subsequent uptake. Cell-surface labeling by CD44 antibodies was likewise significantly diminished following receptor blocking by hyaluronan-LbL nanoparticles (Figure 4c).

In view of the CD44 receptor's role in mediating cell adhesion interactions,[56] we anticipated that the HA-terminal LbL nanoparticles could engage CD44 directly through binding of the receptor, decreasing cell migration. Therefore, we further investigated the effects of hyaluronan-terminal nanoparticles on both 2D and 3D cell migration in a panel of breast carcinoma cells. Sublethal concentrations of hyaluronan-LbL nanoparticles (0.17 nM) significantly diminished cell migration in a 2D gap closure assay, importantly, in a CD44 receptor-selective manner (Figure 4d; Supporting Information Figures S4 and S5). The particles similarly diminished 3D collagen gel transwell invasion, again in a receptor-selective manner, effects which could be recapitulated in part by increasing concentrations of free hyaluronan (Figure 4e). These results are consistent with the notion that CD44-HA binding is a key regulator of cellular adhesion/migration and contact inhibition in cancer cells. Hyaluronic acid, alone for example, has been shown to decrease the invasion of triple-negative breast carcinoma cells into collagen matrices.[57] Tian *et al.* likewise find that contact inhibition and anchorage-dependent growth are controlled by HA–CD44–NF2 signaling in cancer-resistant mole-rats.[58] Interestingly, we find here that HA-LbL nanoparticles can inhibit collagen transwell invasion at $>10^6$-fold lower molar concentrations than free 200 kDa HA (Figure 4e).

We further investigated the role of CD44 *in vivo* using a mouse model; iv-administered hyaluronan-LbL nanoparticles accumulated in MDA-MB-468 breast carcinoma tumor xenografts *ca.* 4.0-fold greater than control nanoparticles of comparable size and charge that were conjugated with dextran sulfate in place of hyaluronan (Figure 5a). Approximately 6% of the initial dose (recovered fluorescence) co-localized with the tumors *ex vivo*, compared with *ca.* 1.5% for the dextran sulfate LbL-coated control. Further, these nanoparticles co-localized with the CD44 receptor in subcutaneous xenograft models of a Ras mutant non-small cell lung carcinoma (A549) following systemic iv administration, as observed in histology from tumor tissue 48 h following nanoparticle administration (Figure 5b),

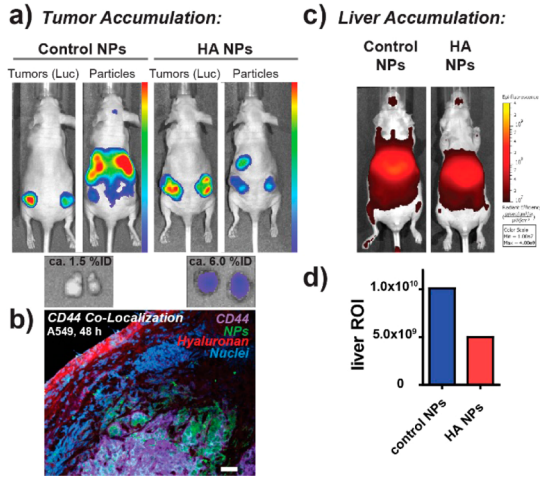

Figure 5. Polysaccharide-LbL nanoparticles target tumors *in vivo*. (a) Tumor co-localization from hyaluronan-LbL nanoparticles compared with dextran sulfate-conjugated control nanoparticles, as imaged by whole-animal bioluminescence/fluorescence imaging (MDA-MB-468/Luc, 72 h). Inset: *ex vivo* analysis of integrated tumor-associated fluorescence. (b) Co-localization of hyaluronan-LbL nanoparticles (green) with CD44 receptor (violet) in histological sections from A549 tumor xenografts following iv injection in tumor-bearing mice (48 h). (c) Accumulation of hyaluronan-LbL nanoparticles and dextran sulfate control nanoparticles in the livers of immunocompetent (non-tumor-bearing) mice following iv injection (48 h) as imaged by whole animal fluorescence. (d) Region-of-interesting analysis of liver-specific accumulation in (c). Scale bar in (b) is 50 μm.

consistent with the notion that hyaluronan-terminal LbL nanoparticles actively target CD44 receptor *in vitro* and *in vivo*. Of note is the significant penetration of nanoparticles through the surrounding stroma into the tumor tissue.

This improved tumor-targeting was accompanied by a 2-fold decrease in liver-specific accumulation, also a key issue for nanoparticle design (Figure 5c,d), again in support of the long blood-stream half-life and stability of the hyaluronan nanoparticles, and the effective steric stabilization afforded by the LbL bilayer at pH 7.4.

CONCLUSIONS

In summary, we describe a LbL nanoparticle architecture capable of active tumor targeting through two unique mechanisms: hypoxic pH-responsive delivery and ligand-directed targeting of the cell-surface receptor CD44 that is overexpressed in many key forms of cancer. The former strategy exploits the dynamic structural stability of multilayered films of weak polyelectrolytes, while the latter utilizes an endogenous polysaccharide, hyaluronan, to direct tissue-specific delivery to cells expressing CD44 receptor, a biomarker for breast and ovarian cancer stem cells. We show that a singular hyaluronan/poly(L-lysine) bilayer adsorbed on a nanoparticle results in hypoxic pH-targeted cellular delivery *in vitro* and co-localization with hypoxia-inducible factor 1 α *in vivo*. Hyaluronan-LbL nanoparticles selectively bound CD44 *in vitro*, diminished cancer cell migration in a receptor-selective manner, and co-localized with CD44 receptor *in vivo*. Because these LbL nanoparticle systems are simple, provide a means of modular design, and can provide enhanced blood half-life[20,26] and enhanced tumor targeting, hyaluronan-LbL nanoparticles are promising candidates for targeted drug delivery to solid tumors for a number of significant cancer types. The ability to target multiple tumor cell populations without the use of additional drug carrier may circumvent resistance from selective pressure while improving safety and treatment outcomes from actively targeted nanomedicines.

MATERIALS AND METHODS

Layer-by-Layer (LbL) Assembly. Nanoparticle LbL assembly was performed as described previously[20] with minor modifications. Briefly, poly(L-lysine) HBr (PLL, 15−30 kDa; Sigma-Aldrich), hyaluronan (HA, 200 kDa; Lifecore), and dextran sulfate sodium salt (20 kDa; Sigma-Aldrich) were used as-received without further modification. All solutions were prepared in PBS ($-Ca^{2+}/-Mg^{2+}$) diluted 100-fold in ultrapure water, adjusted to pH 7.40, and sterile filtered (0.2 μm) immediately prior to use. The 100 nm diameter carboxy-modified polystyrene latex nanospheres were diluted to 0.2 wt %. Nanospheres (2 mg) were added dropwise to a rapidly stirring 45 mL solution of PLL (500 μM) at room temperature (RT) and allowed to stir in dark for 1−2 h. The nanoparticles were recovered by centrifugation (1 h, 15 000 rcf, RT) and diluted to 1 mL. In total, 500 μL of the PLL-conjugated nanoparticles was added dropwise to a rapidly stirring 45 mL solution of HA (10 μM) previously chilled to 4 °C, and the solution was allowed to stir in dark for 30 min at 4 °C. HA-conjugated nanoparticles were recovered by centrifugation (1 h, 15 000 rcf, 4 °C) and stored in dark, as concentrates, at 4 °C within 1 week of use. The 100 nm fluorescent carboxylate-modified polystyrene nanospheres (Life Technologies; Blue 350/440, Red 580/605, Infrared 715/755; Sigma-Aldrich; Orange 481/644) were used as appropriate. Nanoparticle concentration was estimated based on fluorophore absorption λ_{max} and the stock nanoparticle molar concentration as

$$[\text{mol/L}] = \frac{6C \times 10^{15}}{N_A \times \rho \times \pi \times \phi^3} \quad (1)$$

where C is concentration (in g·mL^{-1}), N_A is Avogadro's number 6.022 × 10^{23} mol^{-1}, ρ is density (in g·mL^{-1}) (1.05 for polystyrene), and ϕ is diameter (in μm).

Structural Characterization. Photon correlation spectroscopy and laser Doppler electrophoresis measurements were performed using a Malvern Zetasizer Nano ZS90 particle analyzer (λ = 633 nm, material/dispersant RI 1.590/1.330). TEM was carried out using a JEOL 2100 FEG instrument. EFTEM was performed using a JEOL 2010F TEM equipped with a Gatan imaging filter operating at an accelerating voltage of 200 kV. Samples were prepared by dropcasting particle suspensions onto a TEM grid with a Quantifoil holey carbon support film. Elemental maps were generated at the K edges of carbon (284 eV) and oxygen (532 eV) by using the three window technique and applying the default parameters provided by the Gatan Digital Micrograph software for these elements. EFTEM images were rendered using the Interactive 3D Surface Plot plugin for ImageJ. Measurements were obtained from

ultrapure water or following overnight incubation in phosphate buffered saline (PBS) solutions adjusted using HCl or NaOH. Contact angle measurements were conducted by the Sessile droplet method using a Rame-Hart Contact Angle Goniometer, pH-adjusted PBS buffer, and APTES-modified Si wafers. QCM-D measurements were performed using a Q-Sense E4 instrument (Q-Sense AB, Göthenburg, Sweden), as described previously.[59] The measurement substrate was an amine-modified gold surface, which was prepared by incubating gold-coated sensor crystals (QSX301, Q-Sense AB) in 1 mM 11-amino-1-undecanethiol hydrochloride (Sigma-Aldrich). For QCM-D experiments, 10 mM Tris buffer with 150 mM NaCl (pH 7.5) was first injected in order to obtain a stable baseline, followed by addition of polyelectrolyte solutions (100 $\mu L \cdot min^{-1}$) for 70 min and then static incubation for 20 min. Finally, a buffer wash was performed in the same pH condition and the final change in resonance frequency (Δf) was recorded ($\Delta f_{n=3}/n$ where n is the overtone number corresponding to a 5 MHz AT-cut piezoelectric crystal).

***In Vitro* Experiments.** *Cell Culture.* Hep G2, BT-474, MCF7, SK-BR-3, MDA-MB-231, MDA-MB-468, and A549 cells were obtained from ATCC. A549/Luc and MDA-MB-468/Luc cells were obtained from Cell Biolabs. Cells were subcultured in the supplier's recommended basal medium in a 5% CO_2 humidified atmosphere. All experiments were performed on cells passaged 12−24 h prior.

pH-Dependent Cellular Delivery. Cells were passaged onto 12- or 96-well plates and incubated with 0.17 nM nanoparticle-spiked PBS (Ca^{2+}/Mg^{2+}) of appropriate pH for 3 h. Cell monolayers were washed with PBS, dissociated in 0.25% trypsin−EDTA, and redispersed in PBS containing 1% BSA prior to analysis using a BD LSR II flow cytometer (488 nm ex; 530/30 nm em).

Tumor Spheroids. 3D tumor spheroids were prepared as described previously.[60] Briefly, cells were passaged onto 96-well round-bottom ultralow attachment plates (Corning). After 48−72 h, cell spheroids were transferred onto 18 mm glass coverslips coated with Matrigel GFR (BD) and cell media was supplanted with 50 $\mu L \cdot mL^{-1}$ of Matrigel GFR. Growth media was removed after 48 h and tumor spheroids were washed with PBS (Ca^{2+}/Mg^{2+}) of appropriate pH and incubated for 3 h in PBS containing 0.17 nM nM LbL nanoparticles. Following incubation, cells were rinsed with PBS, fixed in freshly prepared 3.7% formaldehyde (PBS, pH 7.4) for 15 min at RT, and permeablized with 0.1% Triton X-100 (PBS) for 5 min at RT. Coverslips were stained using PBS containing 0.66 μM Alexa Fluor 568 phalloidin (Life Technologies), 4 drops of NucBlue (DAPI; Life Technologies), and 1% BSA for 30 min at RT, then rinsed with PBS prior to mounting with Fluoromount (Sigma) onto no. 0 glass-bottom 35 mm MatTek dishes and imaging using a Nikon 1AR Ultra-Fast Spectral Scanning Confocal Microscope.

CD44-Dependent Cellular Delivery. Cells were transfected with siRNA against human CD44 (SI00299705 FlexiTube siRNA Premix, Quiagen) for 72 h at 25 nM, after which cell monolayers (*ca.* 5×10^5 cells) were incubated with 0.17 nM nanoparticle-spiked PBS (Ca^{2+}/Mg^{2+}) for 3 h, washed with PBS, dissociated in 0.2% EDTA (PBS), pelleted, and labeled with 20 μL of FITC-anti-human CD44 (clone MEM-85; Life Technologies) for 30 min at 4 °C. Cells were recovered by centrifugation (5 min, 600 rcf), fixed in 500 μL of freshly prepared 3.7% paraformaldehyde, and analyzed using a BD LSR II flow cytometer (anti-CD44-FITC: 488 nm ex; 530/30 nm em; nanoparticles: 561 nm ex; 610/20 nm em).

Cell Viability. Cells were passaged onto 96-well plates and incubated with nanoparticle-spiked basal medium for 24 h. Cellular ATP was quantified using CellTiter Glo (Promega).

Migration and Invasion. Scratch-migration assays were performed on confluent 12-well plates using 0.17 nM nanoparticle-spiked complete basal medium and a 1 mL pipet tip. Cell monolayers were monitored using a 5× inverted objective Olympus optical microscope. Collagen-transwell invasion was assessed at the concentrations indicated using a 96-well Boyden chamber (8 μm pores) and complete basal medium as a chemoattractant (CHEMICON Cell Invasion kit). Transwell invasion was quantified after 48 h using CelTiter Glo.

In Vivo Experiments. In total, 5×10^6 A549, MDA-MB-468, or MDA-MB-468/Luc cells (1:1 PBS:Matrigel) were injected subcutaneously into the hindflanks of nude mice (NCR nu/nu, Taconic). Tumors were allowed to form for 2−3 weeks. Nanoparticles (8.3×10^{12} NP·kg^{-1}, 5% glucose) were injected *via* the tail vein into tumor-bearing nude or immunocompetent mice (BALB/c, Taconic). Tumors were harvested after 48 or 72 h and processed by the Swanson Biotechnology Histology Core Facility. Briefly, tumors were formalin-fixed, paraffin-embedded, sectioned (5 μm), deparaffinized, antigen retrieved, and stained using DAPI, biotinylated hyaluronic acid binding protein (Calbiochem), anti-CD44-FITC (Life Technologies), and streptavidin-Alexa Fluor 546 (Life Technologies) or DAPI and anti-HIF1α-fluorescein (R&D Systems). Slides were mounted and imaged using a Nikon 1AR Ultra-Fast Spectral Scanning Confocal Microscope. Whole-animal imaging was performed using a Xenogen IVIS Imaging System (Caliper) with D-luciferin (150 mg kg^{-1} ip, PerkinElmer) as a bioluminescent substrate. These experiments were approved by the Massachusetts Institute of Technology Committee on Animal Care (CAC).

Conflict of Interest: The authors declare no competing financial interest.

Supporting Information Available: Comparative nonspecific and hypoxic-pH specific cell delivery, nanoparticle penetration into 3D tumor spheroids, dose-dependent cell viability, and time-dependent 2D cell migration of CD44 negative breast carcinoma cells. This material is available free of charge *via* the Internet at http://pubs.acs.org.

Acknowledgment. The authors acknowledge generous support from Janssen Pharmaceuticals, Inc., the TRANSCEND partnership, and fellowship support from the NIH (ECD, Kirschstein NRSA 1F32EB017614-02), NSF (SWM), NSERC (KES, NSERC-PDF), and NHMRC (ZJD). This work was supported in part by the Koch Institute Support (core) Grant P30-CA14051 from the NCI, the MIT MRSEC Grant DMR-0819762 from the NSF, the National Research Foundation (NRF-NRFF2011-01), and technical assistance from the MIT Department of Comparative Medicine, Koch Institute Swanson Biotechnology Center, specifically the FACS, Peterson Nanotechnology core, ATWAI, and Tang Histology facilities. The authors are grateful to Officer Sean Collier for his caring service to the MIT community and for his sacrifice.

REFERENCES AND NOTES

1. Eliasof, S.; Lazarus, D.; Peters, C.; Case, R.; Cole, R.; Hwang, J.; Schluep, T.; Chao, J.; Lin, J.; Yen, Y.; *et al.* Correlating Preclinical Animal Studies and Human Clinical Trials of a Multifunctional, Polymeric Nanoparticle. *Proc. Natl. Acad. Sci. U.S.A.* **2013**, *110*, 15127–15132.
2. Akinc, A.; Zumbuehl, A.; Goldberg, M.; Leshchiner, E. S.; Busini, V.; Hossain, N.; Bacallado, S. A.; Nguyen, D. N.; Fuller, J.; Alvarez, R.; *et al.* A Combinatorial Library of Lipid-Like Materials for Delivery of Rnai Therapeutics. *Nat. Biotechnol.* **2008**, *26*, 561–569.
3. Matsumura, Y.; Maeda, H. A New Concept for Macromolecular Therapeutics in Cancer Chemotherapy: Mechanism of Tumoritropic Accumulation of Proteins and the Antitumor Agent Smancs. *Cancer Res.* **1986**, *46*, 6387–6392.
4. Jain, R. K. Transport of Molecules in the Tumor Interstitium: A Review. *Cancer Res.* **1987**, *47*, 3039–3051.
5. Choi, C. H. J.; Alabi, C. A.; Webster, P.; Davis, M. E. Mechanism of Active Targeting in Solid Tumors with Transferrin-Containing Gold Nanoparticles. *Proc. Natl. Acad. Sci. U.S.A.* **2010**, *107*, 1235–1240.
6. Wong, C.; Stylianopoulos, T.; Cui, J.; Martin, J.; Chauhan, V. P.; Jiang, W.; Popović, Z.; Jain, R. K.; Bawendi, M. G.; Fukumura, D. Multistage Nanoparticle Delivery System for Deep Penetration into Tumor Tissue. *Proc. Natl. Acad. Sci. U.S.A.* **2011**, *108*, 2426–2431.
7. Vogelstein, B.; Papadopoulos, N.; Velculescu, V. E.; Zhou, S.; Diaz, L. A.; Kinzler, K. W. Cancer Genome Landscapes. *Science* **2013**, *339*, 1546–1558.
8. Marusyk, A.; Almendro, V.; Polyak, K. Intra-Tumour Heterogeneity: A Looking Glass for Cancer? *Nat. Rev. Cancer* **2012**, *12*, 323–334.

9. Greaves, M.; Maley, C. C. Clonal Evolution in Cancer. *Nature* **2012**, *481*, 306–313.
10. Park, S. Y.; xF; nen, M.; Kim, H. J.; Michor, F.; Polyak, K. Cellular and Genetic Diversity in the Progression of *in Situ* Human Breast Carcinomas to an Invasive Phenotype. *J. Clin. Invest.* **2010**, *120*, 636–644.
11. Maley, C. C.; Galipeau, P. C.; Finley, J. C.; Wongsurawat, V. J.; Li, X.; Sanchez, C. A.; Paulson, T. G.; Blount, P. L.; Risques, R.-A.; Rabinovitch, P. S.; *et al.* Genetic Clonal Diversity Predicts Progression to Esophageal Adenocarcinoma. *Nat. Genet.* **2006**, *38*, 468–473.
12. Bedard, P. L.; Hansen, A. R.; Ratain, M. J.; Siu, L. L. Tumour Heterogeneity in the Clinic. *Nature* **2013**, *501*, 355–364.
13. Caruso, F.; Caruso, R. A.; Mohwald, H. Nanoengineering of Inorganic and Hybrid Hollow Spheres by Colloidal Templating. *Science* **1998**, *282*, 1111–1114.
14. Donath, E.; Sukhorukov, G. B.; Caruso, F.; Davis, S. A.; Möhwald, H. Novel Hollow Polymer Shells by Colloid Templated Assembly of Polyelectrolytes. *Angew. Chem., Int. Ed.* **1998**, *37*, 2201–2205.
15. Shutava, T. G.; Balkundi, S. S.; Vangala, P.; Steffan, J. J.; Bigelow, R. L.; Cardelli, J. A.; O'Neal, D. P.; Lvov, Y. M. Layer-by-Layer-Coated Gelatin Nanoparticles as a Vehicle for Delivery of Natural Polyphenols. *ACS Nano* **2009**, *3*, 1877–1885.
16. Schneider, G.; Decher, G. From Functional Core/Shell Nanoparticles Prepared *via* Layer-by-Layer Deposition to Empty Nanospheres. *Nano Lett.* **2004**, *4*, 1833–1839.
17. Zahr, A.; de Villiers, M.; Pishko, M. Encapsulation of Drug Nanoparticles in Self-Assembled Macromolecular Nanoshells. *Langmuir* **2005**, *21*, 403–410.
18. Agarwal, A.; Lvov, Y.; Sawant, R.; Torchilin, V. Stable Nanocolloids of Poorly Soluble Drugs with High Drug Content Prepared Using the Combination of Sonication and Layer-by-Layer Technology. *J. Controlled Release* **2008**, *128*, 255–260.
19. Poon, Z.; Chang, D.; Zhao, X.; Hammond, P. T. Layer-by-Layer Nanoparticles with a Ph-Sheddable Layer for *in Vivo* Targeting of Tumor Hypoxia. *ACS Nano* **2011**, *5*, 4284–4292.
20. Poon, Z.; Lee, J. B.; Morton, S. W.; Hammond, P. T. Controlling *in Vivo* Stability and Biodistribution in Electrostatically Assembled Nanoparticles for Systemic Delivery. *Nano Lett.* **2011**, *11*, 2096–2103.
21. Hammond, P. T. Polyelectrolyte Multilayered Nanoparticles: Using Nanolayers for Controlled and Targeted Systemic Release. *Nanomedicine* **2012**, *7*, 619–622.
22. Morton, S.; Herlihy, K.; Shopsowitz, K.; Deng, Z.; Chu, K.; Bowerman, C.; Desimone, J.; Hammond, P. Scalable Manufacture of Built-to-Order Nanomedicine: Spray-Assisted Layer-by-Layer Functionalization of Print Nanoparticles. *Adv. Mater.* **2013**, *25*, 4707–4713.
23. Morton, S.; Poon, Z.; Hammond, P. The Architecture and Biological Performance of Drug-Loaded Lbl Nanoparticles. *Biomaterials* **2013**, *34*, 5328–5335.
24. Sukhishvili, S. A. Responsive Polymer Films and Capsules *via* Layer-by-Layer Assembly. *Curr. Opin. Colloid Interface Sci.* **2005**, 10.
25. Luo, R.; Neu, B.; Venkatraman, S. Surface Functionalization of Nanoparticles to Control Cell Interactions and Drug Release. *Small* **2012**, *8*, 2585–2594.
26. Deng, Z. J.; Morton, S. W.; Ben-Akiva, E.; Dreaden, E. C.; Shopsowitz, K. E.; Hammond, P. T. Layer-by-Layer Nanoparticles for Systemic Codelivery of an Anticancer Drug and Sirna for Potential Triple-Negative Breast Cancer Treatment. *ACS Nano* **2013**, *7*, 9571–9584.
27. Morton, S. W.; Shah, N. J.; Quadir, M. A.; Deng, Z. J.; Poon, Z.; Hammond, P. T. Osteotropic Therapy *Via* Targeted Layer-by-Layer Nanoparticles. *Adv. Healthcare Mater.* **2014**, *3* (6), 867–875.
28. Lee, J. B.; Hong, J.; Bonner, D. K.; Poon, Z.; Hammond, P. T. Self-Assembled RNA Interference Microsponges for Efficient Sirna Delivery. *Nat. Mater.* **2012**, *11*, 316–322.
29. Ye, C.; Drachuk, I.; Calabrese, R.; Dai, H.; Kaplan, D.; Tsukruk, V. Permeability and Micromechanical Properties of Silk Ionomer Microcapsules. *Langmuir* **2012**, *28*, 12235–12244.
30. Tan, Y.; Mundargi, R.; Chen, M.; Lessig, J.; Neu, B.; Venkatraman, S.; Wong, T. Layer-by-Layer Nanoparticles as an Efficient Sirna Delivery Vehicle for Sparc Silencing. *Small* **2014**, *10*, 1790–1798.
31. Caruso, F.; Spasova, M.; Susha, A.; Giersig, M.; Caruso, R. A. Magnetic Nanocomposite Particles and Hollow Spheres Constructed by a Sequential Layering Approach. *Chem. Mater.* **2001**, *13*, 109–116.
32. Drachuk, I.; Gupta, M. K.; Tsukruk, V. V. Biomimetic Coatings to Control Cellular Function through Cell Surface Engineering. *Adv. Funct. Mater.* **2013**, *23*, 4437–4453.
33. Wilson, J. T.; Cui, W.; Kozlovskaya, V.; Kharlampieva, E.; Pan, D.; Qu, Z.; Krishnamurthy, V. R.; Mets, J.; Kumar, V.; Wen, J.; *et al.* Cell Surface Engineering with Polyelectrolyte Multilayer Thin Films. *J. Am. Chem. Soc.* **2011**, *133*, 7054–7064.
34. Mendelsohn, J.; Barrett, C.; Chan, V.; Pal, A.; Mayes, A.; Rubner, M. Fabrication of Microporous Thin Films from Polyelectrolyte Multilayers. *Langmuir* **2000**, *16*, 5017–5023.
35. Harris, J. J.; Bruening, M. L. Electrochemical and *in Situ* Ellipsometric Investigation of the Permeability and Stability of Layered Polyelectrolyte Films. *Langmuir* **2000**, *16*, 2006–2013.
36. Petrov, A. I.; Antipov, A. A.; Sukhorukov, G. B. Base-Acid Equilibria in Polyelectrolyte Systems: From Weak Polyelectrolytes to Interpolyelectrolyte Complexes and Multilayered Polyelectrolyte Shells. *Macromolecules* **2003**, *36*, 10079–10086.
37. Jain, R. K.; Stylianopoulos, T. Delivering Nanomedicine to Solid Tumors. *Nat. Rev. Clin. Oncol.* **2010**, *7*, 653–664.
38. De Bock, K.; Mazzone, M.; Carmeliet, P. Antiangiogenic Therapy, Hypoxia, and Metastasis: Risky Liaisons, or Not? *Nat. Rev. Clin. Oncol.* **2011**, *8*, 393–404.
39. Hashimoto, D.; Hirota, M.; Yagi, Y.; Baba, H. Hyaluronate Carboxymethylcellulose-Based Bioresorbable Membrane (Seprafilm) Reduces Adhesion under the Incision to Make Unplanned Re-Laparotomy Safer. *Surg. Today* **2012**, *42*, 863–867.
40. Al-Hajj, M.; Wicha, M.; Benito-Hernandez, A.; Morrison, S.; Clarke, M. Prospective Identification of Tumorigenic Breast Cancer Cells. *Proc. Natl. Acad. Sci. U.S.A.* **2003**, *100*, 3983–3988.
41. Alvero, A. B.; Chen, R.; Fu, H.-H.; Montagna, M.; Schwartz, P. E.; Rutherford, T.; Silasi, D.-A.; Steffensen, K. D.; Waldstrom, M.; Visintin, I.; *et al.* Molecular Phenotyping of Human Ovarian Cancer Stem Cells Unravels the Mechanisms for Repair and Chemoresistance. *Cell Cycle* **2009**, *8*, 158–166.
42. Zhang, S.; Balch, C.; Chan, M. W.; Lai, H.-C.; Matei, D.; Schilder, J. M.; Yan, P. S.; Huang, T. H.-M.; Nephew, K. P. Identification and Characterization of Ovarian Cancer-Initiating Cells from Primary Human Tumors. *Cancer Res.* **2008**, *68*, 4311–4320.
43. Ricardo, S.; Vieira, A.; Gerhard, R.; Leitão, D.; Pinto, R.; Cameselle-Teijeiro, J.; Milanezi, F.; Schmitt, F.; Paredes, J. Breast Cancer Stem Cell Markers Cd44, Cd24 and Aldh1: Expression Distribution within Intrinsic Molecular Subtype. *J. Clin. Pathol.* **2011**, *64*, 937–946.
44. Choi, K.; Yoon, H.; Kim, J.-H.; Bae, S.; Park, R.-W.; Kang, Y.; Kim, I.-S.; Kwon, I.; Choi, K.; Jeong, S.; *et al.* Smart Nanocarrier Based on Pegylated Hyaluronic Acid for Cancer Therapy. *ACS Nano* **2011**, *5*, 8591–8599.
45. Ganesh, S.; Iyer, A.; Gattacceca, F.; Morrissey, D.; Amiji, M. *In Vivo* Biodistribution of Sirna and Cisplatin Administered Using Cd44-Targeted Hyaluronic Acid Nanoparticles. *J. Controlled Release* **2013**, *172*, 699–706.
46. Cohen, K.; Emmanuel, R.; Kisin-Finfer, E.; Shabat, D.; Peer, D. Modulation of Drug Resistance in Ovarian Adenocarcinoma Using Chemotherapy Entrapped in Hyaluronan-Grafted Nanoparticle Clusters. *ACS Nano* **2014**, *8*, 2183–2195.
47. Scott, J. E. Supramolecular Organization of Extracellular Matrix Glycosaminoglycans, *In Vitro* and in the Tissues. *FASEB J.* **1992**, *6*, 2639–2645.
48. Burke, S.; Barrett, C. pH-Responsive Properties of Multilayered Poly(L-lysine)/Hyaluronic Acid Surfaces. *Biomacromolecules* **2003**, *4*, 1773–1783.

49. Bauer, S.; Arpa-Sancet, M.; Finlay, J.; Callow, M.; Callow, J.; Rosenhahn, A. Adhesion of Marine Fouling Organisms on Hydrophilic and Amphiphilic Polysaccharides. *Langmuir* **2013**, *29*, 4039–4047.
50. Mueller, M.; Fusenig, N. Friends or Foes—Bipolar Effects of the Tumour Stroma in Cancer. *Nat. Rev. Cancer* **2004**, *4*, 839–849.
51. Shiratori, S. S.; Rubner, M. F. pH-Dependent Thickness Behavior of Sequentially Adsorbed Layers of Weak Polyelectrolytes. *Macromolecules* **2000**, *33*, 4213–4219.
52. Burke, S. E.; Barrett, C. J. Swelling Behavior of Hyaluronic Acid/Polyallylamine Hydrochloride Multilayer Films. *Biomacromolecules* **2005**, *6*, 1419–1428.
53. Nel, A. E.; Mädler, L.; Velegol, D.; Xia, T.; Hoek, E. M. V.; Somasundaran, P.; Klaessig, F.; Castranova, V.; Thompson, M. Understanding Biophysicochemical Interactions at the Nano-Bio Interface. *Nat. Mater.* **2009**, *8*, 543–557.
54. Wilson, W.; Hay, M. Targeting Hypoxia in Cancer Therapy. *Nat. Rev. Cancer* **2011**, *11*, 393–410.
55. Olaku, V.; Matzke, A.; Mitchell, C.; Hasenauer, S.; Sakkaravarthi, A.; Pace, G.; Ponta, H.; Orian-Rousseau, V. C-Met Recruits Icam-1 as a Coreceptor to Compensate for the Loss of Cd44 in Cd44 Null Mice. *Mol. Biol. Cell* **2011**, *22*, 2777–2786.
56. Zöller, M. Cd44: Can a Cancer-Initiating Cell Profit from an Abundantly Expressed Molecule? *Nat. Rev. Cancer* **2011**, *11*, 254–267.
57. Lopez, J.; Camenisch, T.; Stevens, M.; Sands, B.; McDonald, J.; Schroeder, J. Cd44 Attenuates Metastatic Invasion During Breast Cancer Progression. *Cancer Res.* **2005**, *65*, 6755–6763.
58. Tian, X.; Azpurua, J.; Hine, C.; Vaidya, A.; Myakishev-Rempel, M.; Ablaeva, J.; Mao, Z.; Nevo, E.; Gorbunova, V.; Seluanov, A. High-Molecular-Mass Hyaluronan Mediates the Cancer Resistance of the Naked Mole Rat. *Nature* **2013**, *499*, 346–349.
59. Cho, N.-J.; Frank, C.; Kasemo, B.; Höök, F. Quartz Crystal Microbalance with Dissipation Monitoring of Supported Lipid Bilayers on Various Substrates. *Nat. Protoc.* **2010**, *5*, 1096–1106.
60. Vinci, M.; Gowan, S.; Boxall, F.; Patterson, L.; Zimmermann, M.; Court, W.; Lomas, C.; Mendiola, M.; Hardisson, D.; Eccles, S. Advances in Establishment and Analysis of Three-Dimensional Tumor Spheroid-Based Functional Assays for Target Validation and Drug Evaluation. *BMC Biol.* **2012**, *10*, 29.